Data-driven large-scale genomic analysis reveals an intricate phylogenetic and functional landscape in J-domain proteins

Duccio Malinverni[a,+,*], Stefano Zamuner[b*], Mathieu E. Rebeaud[b], Alessandro Barducci[c], Nadinath B. Nillegoda[d,e,1], Paolo De Los Rios[b,f,1]

[a] Department of Structural Biology and Center for Data Driven Discovery, St Jude Children's Research Hospital, Memphis, TN, USA

[b] Institute of Physics, School of Basic Sciences, École Polytechnique Fédérale de Lausanne – EPFL, CH-1015 Switzerland.

[c] Centre de Biologie Structurale (CBS), INSERM, CNRS, Université de Montpellier, Montpellier, France.

[d] Australian Regenerative Medicine Institute (ARMI), Monash University, Melbourne, Victoria, Australia

[e] Centre for Dementia and Brain Repair at the Australian Regenerative Medicine Institute, Monash University, Melbourne, Victoria, Australia

[f] Institute of Bioengineering, School of Life Sciences, École Polytechnique Fédérale de Lausanne – EPFL, CH-1015 Switzerland.

[+] Work done while at EPFL and MRC Laboratory of Molecular Biology, Cambridge, UK

[*] The authors contributed equally to this work

[1] Correspondence: nadinath.nillegoda@monash.edu , paolo.delosrios@epfl.ch

Abstract

The 70 kDalton Heat shock protein (Hsp70) chaperone system is emerging as a central hub of the proteostasis network that helps maintain protein homeostasis in all organisms. The recruitment of Hsp70 to perform a vast array of different cellular functions is regulated by a family of co-chaperones known as J-domain proteins (JDP) that bear a small namesake J-domain, which is required to interact and drive the ATPase cycle of Hsp70s. Both prokaryotic and eukaryotic JDPs display staggering diversity in domain architecture (besides the ubiquitous J-domain), function, and cell localization. On the contrary, a relatively small number of Hsp70 paralogs exist in cells, suggesting a high degree of specificity, but also promiscuity, in the partnering between JDPs and Hsp70s. Very little is known about the JDP family, despite their essential role in cellular proteostasis, development, and the link to a broad range of human diseases. The number of JDP gene sequences identified across all kingdoms as a consequence of advancements in sequencing technology has exponentially increased, where it is now beyond the ability of careful manual curation. In this work, we first provide a broad overview of the JDP repertoire accessible from public databases, and then we use an automated classification scheme, based on Artificial Neural Networks (ANNs), to demonstrate that the sequences of J-domains carry sufficient discriminatory information to recover with high reliability the phylogeny, localization, and domain

composition of the corresponding full-length JDP. By harnessing the interpretability of the ANNs, we find that many of the discriminatory sequence positions match to residues that form the interaction interface between the J-domain and Hsp70. This reveals that key residues within the J-domains have coevolved with their obligatory Hsp70 partners to build chaperone circuits for specific functions in cells.

Keywords: J-domain proteins, Hsp40 Co-chaperones, Protein Homeostasis, Large-scale Data Analysis, Artificial Neural Networks

Introduction

Hsp70 is an essential and highly ubiquitous chaperone involved in a wide variety of constitutive and stress-related cellular processes, including the promotion of protein folding[1,2], the prevention and reversal of the formation of cytotoxic aggregates[3–6], the import of polypeptides into cell compartments [7,8], driving the (dis)assembly of oligomeric protein complexes[9–11] , the regulation of protein activity[12] and the targeting of terminally damaged proteins for degradation[13–15]. Underlying these diverse functions is the fundamental ability of Hsp70 to bind substrate proteins upon a conformational change that depends on the nature of the bound nucleotide, which alternates between ATP and ADP. This biochemical cycle is stringently regulated by J-domain containing proteins (JDPs) that, together with the substrate, accelerate ATP hydrolysis in Hsp70s by orders of magnitude[16,17], which results in ultra-affinity binding, namely a significant, non-equilibrium enhancement of the Hsp70 affinity for its substrates[18]. Subsequently, Hsp70 nucleotide exchange factors (NEFs) bind and accelerate ADP release, thus allowing rebinding of ATP and client protein release[19] (Fig.1A).

All members of the JDP family invariably contain a J-domain, the namesake domain which is ~63 residue-long. The J-domain is formed by a well-defined arrangement of four alpha helices (Fig.1B) with a highly-conserved Histidine-Proline-Aspartate (HPD) motif between helices 2 and 3. The helix II-HPD-helix III motif forms the primary interface for the interaction and stimulation of ATP hydrolysis in Hsp70[16,17,20–23]. The remaining subdomains help target JDPs to specific locations, client proteins, or protein conformations (*e.g.* unfolded, misfolded, or aggregated polypeptides), thereby recruiting the action of Hsp70s to selected substrates[24,25].

A classification scheme for JDPs has been suggested based on the overall domain architecture, resulting in three main classes[24,26–28]. Class A JDPs share the domain architecture of the prototypical DnaJ member of *Escherichia coli*. Members of this class consist of an N-terminal J-domain, followed by a glycine and phenylalanine (G/F) rich region and two successive C-terminal β-sandwich domains (CTDs), with a zinc-finger-like region (ZFLR) domain protruding from the first CTD, and are terminated by a short dimerization domain at the C-terminal (Fig.1C). The presence of an N-terminal J-domain fused with a

G/F region was used as the primary domain signature to segregate some of the remaining JDPs to form the so-called class B. This relatively loose classification step, probably stemming from limited availability of JDP sequences at the conception of this class, comprises both the "canonical" type members that share the same domain architecture of class A with the exception of missing the ZFLR (Fig.1D), alongside more diverse ones, that are characterized by an N-terminal J-domain followed by a G/F rich region-only[27]. The G/F-rich region of both classes is typically considered largely unstructured. All the JDPs belonging to class A and some of the ones belonging to class B (also known collectively as Hsp40s owing to their approximate 40 kDa molecular mass) constitutively form homo-dimers through the C-terminal dimerization domain (Fig.1C and D), and bind a large variety of unfolded, misfolded, or aggregated substrates through one or multiple interaction sites located on their CTDs and, possibly for class A, on the ZFLR[29,30]. Thus, class A and B JDPs help recruit Hsp70s to their misfolded/aggregated substrates and contribute to the crowding of Hsp70s on the substrate[4]. In contrast, class C JDPs display a high variability in domain architectures (two examples are shown in Fig.1E and F) and have been historically classified by what they are not, namely neither A nor B, rather than by what they are. Indeed, while members of class C represent the vast majority of JDPs, and intervene in a wide range of unrelated biological pathways (*e.g.* auxilin, which is involved in clathrin cage disassembly; Hsc20, which regulates FeS cluster biogenesis; Sec63, which promotes post-translational protein import in the ER; Zuotin, which assists protein translation), they share with each other little or no common functional or phylogenetic features, except for the presence of a J-domain.

Here, we leveraged the recent exponential growth in genomic data and the improvements in homology detection tools to explore the relations between JDP sequences and their phylogenetic and functional classification at various resolutions. In particular, we focus on class C JDPs, and uncover several subclasses based on most common domain architectures. We then used Artificial Neural Networks (ANNs) to show that even the relatively short and simple sequences of the J-domains generally carry sufficient phylogenetic and functional signatures that may modulate JDP-Hsp70 chaperone circuits *in vivo.* These unique signatures reliably identify the architecture of the corresponding full-length JDP, its cell location, and the taxonomic clade. These findings allowed us to use amino acid sequence variations embedded in the J-domain to develop an ANN-based automated solution to curate existing and new JDP sequences reported in various organisms with high precision. By further identifying the residues that are most important for classification, we pinpointed the structural positions where the class- and organism-specific signatures are located.

From a more general perspective, we highlight how the combination of interpretable large-scale sequence analysis techniques and coarse-grained annotations can unlock the wealth of information that would otherwise remain hidden in exponentially growing, and thus manually unmanageable, sequence databases.

Results

Construction of an extensive annotated J-domain protein sequence dataset

The number of deposited JDP sequences in the UniProt repository[31] has been exponentially growing over the past two decades, increasing by an order of magnitude every 6-7 years (Fig.2A), ranging from 10^3 in year 2003 to 10^5 in year 2018, and projected to reach 10^6 sequences in years 2024-2025 and 10^7 in the early 2030s. Using stringent homology search criteria, we extracted a total of 223'124 JDP sequences from existing genome databases (see Methods). The associated annotations allowed us to assign all JDPs to different phylogenetic classes at various taxonomic levels. Using sequence domain models from the Pfam database[32], we further characterized the domain composition of full-length sequences, assigning to each JDP a tag describing the domain architecture of the protein. Protein-localization prediction algorithms were used to infer the most probable organelle of residence of eukaryotic JDPs (see Methods). This compound procedure allowed us to assign each JDP sequence in the dataset a set of *ground-truth* attributes comprising phylogenetic, architectural, and cellular localization features. In this context, the characteristics that describe, for instance, human DNAJA1 are: a) sequence composition, b) class (e.g. class A JDP based on the full-length domain composition), c) phylogeny (e.g. eukaryotic/metazoan/mammalian protein), and d) cell location (e.g. predominantly cytoplasmic).

The correct identification and proper functional assignment of such a plethora of JDPs is incompatible with any careful manual curation. Instead, the rapidly growing size of the JDP repertoire will require rigorous, but automated characterization and analysis approaches trained on extensive datasets endowed with some reliable ground truth, defined according to different, complementary criteria. We provide such a dataset containing a comprehensive collection of richly annotated repertoire of JDPs in this work. This collection allowed us to investigate the ability of automated approaches to extract and rationalize the information it contains, while gaining new insights into this complex cochaperone family.

Overall characterization of the diversity of the J-domain protein dataset

Based on the overall domain composition of JDPs, the three established functional classes were clearly identifiable: Class A and class B (members with the canonical Hsp40 domain architecture, Figs.1C and D) represented 24.4% and 13% of the dataset, respectively (Fig.2B), with the remaining JDPs (62.6%, corresponding to ~140’000 sequences) assigned to class C. Approximately half of them (78’282) have a domain-architecture consisting of, according to the Pfam-based annotation, only the J-domain (Fig.2F). In some cases, this is due to the absence of any additional domains in the protein, while in others, it could be due to the inability of the Markov models used to effectively recognize variations of existing or potentially new domains. This is likely the case for DNAJB2, which has two ubiquitin binding modules (UIMs)[33,34] that are nonetheless not detected using the Pfam Markov models. These observations clearly require curation not at the level of amino acid sequences, but at the level of the

accuracy/coverage of the models. JDPs annotated with a single J-domain were slightly enriched in eukaryotic organisms (Supplementary Fig.1A) but found uniformly throughout all predicted subcellular locations (Supplementary Fig.1B). The full protein length distribution for JDPs annotated with a single J-domain was significantly shorter than for (annotated) JDPs consisting of multi-domain architectures (Supplementary Fig.1E). However, we also found a significant number of JDPs annotated with a single J-domain, but with relatively long protein sequences, which highlights the finite accuracy of automated domain annotation procedure.

Collectively, the 12 most populated domain architectures (including class A and B JDPs) comprised approximately 90% of the total dataset (196'719 sequences). Visual inspection of class A and B JDP sequences showed that beyond the clear difference due to the presence of the ZFLR, we could also distinguish sequences belonging to the two classes by the composition of their G/F-rich regions. Here, we show that the amino acid profiles of residues in the G/F regions of classes A and B are remarkably different, with the G/F-rich regions of class A showing a more marked segregation of phenylalanine, arginine, glycine and glutamate residues compared to those of class B JDPs (Fig.2C and D). This was quantitatively confirmed by a simple linear classification model which showed that the amino acid sequences (unaligned) of the G/F region alone were able to successfully discriminate JDPs of class A and B (classification accuracy of ~95%, see FigS7 and Methods for details). These significant differences in amino acid compositions suggest that at least parts of the G/F rich region could have different functions beyond being a simple flexible linker. Recent observations show that in some class B members, a small helix in the G/F region docks with the J-domain, likely with functional consequences[35–38]. Furthermore, it was shown that some JDPs could, to a certain degree, undergo liquid-liquid phase separation with the help of the G/F regions[39].

In agreement with previous observations[25], class C members dominated the dataset (Fig.2B) mainly due to their overwhelming abundance in eukaryotes (Fig.2E and Supplementary Fig.2A for a more detailed analysis of class C abundance in the dataset). There were 1945 different architectures present in class C, which were built from 1558 distinct domains. Most of these domains were often classified as Domain of Unknown Function (DUFs) and showed little to no co-occurrence with the most common domains (Supplementary Fig.3). The only notable exceptions are JDPs containing multiple repeats of tetratricopeptides (TPR) associated with several different Pfam families (in Fig.2F and Supplementary Fig.3 all these TPR domains are collected in a single group). Inspection of the architectures of the most frequently observed JDP domains within class C revealed a very disparate phylogenetic makeup (Fig.2F). For instance, JDPs of the bacterial (*E. coli*) DjlA family, which formed the most abundant class C-subtype architecture, are present only in bacteria. The HscB family (human DNAJC20, Fig.1F), which participates in iron-sulfur cluster assembly pathway, is present in both prokaryotes and eukaryotes. Others, such as the yeast Sec63 (DNAJC18) localized in the endoplasmic reticulum (ER), (which shares almost the same domain composition as DNAJB12 and DNAJB14), DNAJC11

183 (DUF3995), and DNAJC3/ DNAJC7 were found only in eukaryotes. Some highly represented
184 architectures obeyed an even finer phylogenetic distribution, with Djp1/Caj1, JJJ1, and JJJ3 (yeast
185 names) present only in yeast (*e.g.* in *S. cerevisiae*). These observations across all organisms, mirror and
186 greatly expand recent observations made on bacterial and phage JDPs that also revealed the diversity
187 of architectures among class C JDPs, more often than not with yet unknown cellular functions[40].

188 We then analyzed the predicted subcellular localization of JDPs to assess if the classes are differently
189 represented in various cellular compartments. Analysis of the organellar makeup of the dataset revealed
190 that mitochondrial JDPs were mainly of class A and C (Supplementary Fig.2B) while mitochondrial
191 class B JDPs were only about 10% of the class A JDPs, compatible with the precision of the localization
192 algorithm itself (see Methods). This suggested that mitochondrial JDPs largely belong to class A, with
193 some exceptions that must be manually inspected. ER-localized JDPs showed an intriguing class
194 distribution. In addition to several class C JDPs, the ER contains a resident class A/B-type JDP, which
195 in fungi (and some other unicellular eukaryotes such as amoebas) is a canonical class A, while in
196 metazoa and plants (DNAJB11/Erdj3) it belongs to class B due to the lack of a ZFLR. A closer
197 inspection revealed that, instead of the customary ZFLR, a non-canonical cysteine-rich region (which
198 we call here *pseudoZFLR*) is generally found in these class B-like members. The pseudoZFLR regions
199 display regularity and high degree of similarity in plants and metazoa (Fig.2G), with only two Cys pairs.
200 The first Cys pair shows a highly conserved CNC motif, while the 2nd pair has the two cysteines
201 separated by two residues. This motif represents an interesting evolutionary conundrum, given that the
202 most accepted view of the evolution of eukaryotes posits that the divergence in opisthokonts, between
203 fungi and metazoan, took place after the split from plants.

204 ***J-domain sequences contain functional and phylogenetic information at multiple scales***

205 Organisms ranging from viruses to prokaryotes to eukaryotes rely on multiple pairs of Hsp70s and JDPs
206 to support various biological activities. What largely remains unclear is how a particular JDP recognizes
207 its partner Hsp70, an interaction that is largely mediated by the J-domain. It has been speculated for
208 many years that the specificity should thus be encoded in the sequences of both partners, calling into
209 question the degree to which the J-domains can be interchanged between different JDPs with minimal
210 consequences for its primary function. In fact, not all J-domains interact indifferently with Hsp70s.
211 Exchanges of J-domains between two JDPs frequently result in non-functional chimeras, suggesting
212 that there is selectivity in the pairing of JDPs and Hsp70s[28,41–45]. Evolutionary and functional factors
213 such as phylogeny, interactions with different Hsp70 paralogs, as well as the colocalization of J- and
214 non-J-domains in the same polypeptide, may have left traces in the sequence of the J-domain. If this
215 was the case, the sequence of a J-domain alone should carry relevant information about the overall JDP
216 to which it belongs.

217 To test this hypothesis and provide evidence to support that the sequences of J-domains carry a rich
218 source of disparate evolutionary and functional signatures, we first extracted and aligned 223'124 J-

219 domain sequences from our JDP repertoire (see Methods for detailed procedure). We then used the
220 unsupervised UMAP algorithm[46] to provide a (non-linear) projection of the sequences in two
221 dimensions, allowing for their direct visual inspection (Fig.3; see Methods). The projections revealed
222 that the J-domain sequences are gathered in clusters, and that the different groups, highlighted by
223 different colors, often associated well with various classification schemes, such as their *i*) A, B, or C
224 class (Fig.3A), *ii*) bacteria rather than eukaryotes (Fig.3B) *iii*) various C subclasses (only the five more
225 abundant ones are represented in Fig.3C for sake of clarity). To highlight the finer signatures that are
226 encoded in the J-domain sequences, we focus on HscB. Besides being well-clustered according to the
227 previous criteria (circles in Figs.3A, B, and C), the HscB sequences from fungi, metazoa and plants
228 were also clearly individually well-grouped (Fig.3D). Thus, different and non-dependent layers of
229 information are simultaneously encoded in the sequences of the J-domains, both to finer phylogenetic
230 levels or for other criteria, such as subcellular localization (Supplementary Fig.4).

231 ***Classification of J-domains by artificial neural networks***

232 Next, we used an approach based on artificial neural networks (ANN) to find the detailed determinants
233 in J-domain sequences that underpin different classifications. We focus on a few broad category
234 discriminations, namely:

235 - Class A *vs.* class B (henceforth referred to as A/B);
236 - A *vs.* B *vs.* C (henceforth referred to as A/B/C);
237 - 12 different architectural classes, including the architectures of classes A and B JDP, the 9 most
238 populated C subclasses (excluding JDPs containing only the DnaJ domain) and an additional
239 "Other" class generically comprising all remaining JDPs (again not including JDPs containing
240 only DnaJ domain) (henceforth referred to as Arch12). The 12 architectural classes in the Top12
241 task are thus "ClassA (DnaJ-DnaJ_C-DnaJ_CXXCXGXG", "Class B (DnaJ-DnaJ_C)",
242 "TerB_DnaJ", "DnaJ-TPR", "DnaJ-HSCB_C", "DnaJ-DUF1977", "DnaJ-DnaJ-X", "DnaJ-
243 DnaJ_like_C11_C", "DnaJ-zf-CSL", "DnaJzf-C2H2_jaz", "DnaJ_Sec63", "Other";
244 - Bacteria *vs.* eukaryotes *vs.* archaea *vs.* Viruses (henceforth referred to as Bac/Euk/Arch/Vir);
245 - Alphaproteobacteria *vs.* gammaproteobacteria *vs.* firmicutes *vs.* metazoa *vs.* plants *vs.* fungi
246 (henceforth referred to as Phylo);
247 - Endoplasmic reticulum *vs.* mitochondria *vs.* plastids (henceforth referred to as Localization).

248 Although these different groupings are far from exhaustive, we chose them as representatives of both
249 complementary and orthogonal criteria.

250 ANNs are often considered black-boxes with high performance for their assigned tasks, but poor
251 interpretability. To circumvent this limitation, we employed a mathematical approach that makes ANNs
252 interpretable, thus gaining a deeper insight into the information encoded in J-domain sequences. The
253 sequence of operations performed by ANNs is shown in Fig.4A (and further detailed in the Methods).

The nodes (neurons) of the input layer receive the J-domain sequences in a suitable mathematical encoding, $\{x_i\}$. The nodes of the first *hidden* layer receive *affine transformations* $y_j^{[1]}$ of the input values, with weights $\left\{w_{ji}^{[in,1]}\right\}$ and offsets $\left\{b_j^{[in,1]}\right\}$: $y_j^{[1]} = \sum_i w_{ji}^{[in,1]} x_i + b_j^{[in,1]}$ (subscripts indicate the connected nodes in the two layers, and the superscripts in the square brackets indicate corresponding layers). The output of the first hidden layer is then computed by applying a non-linear function to each of the $\left\{y_j^{[1]}\right\}$, resulting in a set of values $\left\{f\left(y_j^{[1]}\right)\right\}$, which is then passed to the nodes of the second hidden layer after undergoing the same set of operations. This procedure is repeated from layer to layer until the transferred values reach the nodes of the output layer that are in numbers equal to the different classes to be recognized (*e.g.* 3 output nodes for A/B/C, or 13 output nodes for Arch12). The output values are eventually transformed into the predicted probability that the input sequence $\{x_i\}$ belongs to each given class.

The training of the ANNs consisted in progressively modifying the network parameters (weights and offsets) until the output probabilities of the sequences of the dataset were, on average, as similar as possible to ground truths established previously (Fig.4B). For example, in the A/B/C classification task, the J-domain of HscB belongs to class C with certainty, corresponding to the probabilities (0,0,1), which is the set of values that the ANN should reproduce. To prevent the networks from overfitting by learning each sequences labels, the dataset was split into two parts. One part was used for training, while the other (test set) was used to check the predictions on sequences not seen during the learning phase. An ANN could be reliably used as a classification tool only if the performance on the training set was comparable to that on the test set, which we observed.

For each of the tasks (A/B, A/B/C, *etc.*), the output probabilities were used as coordinates for a low-dimensional representation of the dataset, similarly to the analysis performed in Fig.3. As an example, this kind of representation is shown in Fig.4C for the classification task A/B/C (including a further reduction in dimensionality from three to two dimensions using the UMAP algorithm), providing evidence that the ANN had found information embedded in J-domain sequences that allowed it to easily distinguish the three classes.

To move beyond the visual (but not quantitative) appraisal of the performance of the ANNs, we computed their *confusion matrices* (Fig.4D), which report the misclassification of each category with respect to their *ground truth*. An example is shown in Fig.4D where J-domains belonging to JDPs of class A were correctly classified 96.7% of the times, and misclassified as class B or C members only 2.6% and 0.7% of the times, respectively. Similarly, class B J-domains were classified according to their ground truth 91.6% of the times. Overall, the performance of the ANNs for all classification tasks was excellent (Supplementary Fig.5). The only classification task that was slightly less accurate was localization, although it is important to recall that the accuracy in this case was compatible with the prediction accuracy of the algorithms used to define the localization ground truth (see Methods).

289 Overall, the success of our ANN classification approach highlights that a myriad of phylogenetic and
290 functional signatures is indeed encoded in J-domain sequences alone and that this methodology can be
291 used to tell J-domains apart from each other depending on different, possibly orthogonal, criteria such
292 as phylogeny, subcellular localization, and domain organization. The co-evolution of J-domain
293 sequences with the full protein architecture has also been recently reported, albeit restricted to bacterial
294 genomes[40].

295 We finally used our trained ANNs to predict the A, B, and C classes, as well as the Archs12 labels of
296 the 78'282 JDPs with an annotated domain architecture composed of a single DnaJ. Note again that
297 none of these ~78'000 sequences were used during network training. The ANNs correctly classified
298 vast majority of these as class C JDPs. Interestingly, more than 60% of these singleton JDPs were
299 classified as "Other" in the Archs12 task, implying that the network has probably learned that the
300 divergent signatures of these JDPs are dissimilar from the other classes used to learn this task. The
301 second and third most predicted classes on this set correspond to class A and B JDPs (~9% and ~17%
302 respectively), which is likely due to them being the most abundant JDPs in the training set. Collectively,
303 these results seem to indicate that a substantial fraction of JDPs with the J-domain alone, or together
304 with unannotated co-domains, exist, and that these form a (probably heterogenous) divergent clade of
305 J-domains.

306 ***Structural characterization of the most relevant discriminative sequence positions***

307 Next, we used the interpretability of the ANNs to identify the sequence positions that were most relevant
308 for each classification task (see Methods) by assigning them a *relevance score*[47]. We found that although
309 several of the sequence positions were expectedly task-specific, some were ubiquitously important for
310 all tasks (heatmap in Fig.5A). In general, the average score of the relevance for different tasks
311 highlighted the positions that were most relevant to classify J-domains. Thus, we map the five top
312 scoring positions in the structure of the J-domain of *E. coli* DnaJ in the DnaJ-DnaK chaperone complex
313 (*E. coli* Hsp70) chaperone complex (Fig.5B; the five most relevant positions for each classification task
314 are shown in Supplementary Fig.6)[21]. Importantly, we observed that the five top-scoring positions,
315 located at helix II and III of the J-domain, overlapped with the interaction surface between the J-domain
316 of DnaJ and DnaK[21]. This is an intriguing result, because at no step of our analysis we used information
317 about the binding of J-domains to Hsp70. It is thus tempting to hypothesize that the various, possibly
318 orthogonal, classifications are successful because, among other factors, J-domains coevolved together
319 with Hsp70 in a concerted phylogenetic and functional divergence. We presume that these positions
320 likely facilitate modulation of the interaction between J-domain and Hsp70, and HPD-dependent tuning
321 of Hsp70's ATPase activity.

322 ***Classification of J-domain Proteins according to their J-domains***

323 Next, we employed the ANNs as class predictors for the human JDPs. We first excluded all human
324 JDPs, together with those of other model organisms (see Methods) from the training set to prevent any

325 bias during the learning process. In Table 1, we report the probabilities attributed to each human J-
326 domain with respect to a given class or architectural group.

327 The J-domains of human class A (DNAJA1-4) and "canonical" class B (DNAJB1, DNAJB4, DNAJB5)
328 were correctly classified according to the tasks A/B, A/B/C and Arch12 (Table 1 and Supplementary
329 Table 2 for the task A/B), confirming that the ANNs were able to reliably learn their characteristics
330 during the training phase. A more specific discussion is warranted for DNAJB11 and DNAJB13, whose
331 J-domains were consistently classified as class C according to the A/B/C classification task. They were,
332 however, correctly classified by the Arch12 task as either "Other" (DNAJB11) or recognized as
333 canonical class B in the Arch12 task (Table 1). These results suggest that DNAJB11 and DNAJB13,
334 despite a likely class B origin, have further diverged enough that their sequences do not fully conform
335 to the majority of class B JDPs.

336 Class B JDPs with non-canonical architectures (DNAJB2, DNAJB3, DNAJB6, DNAJB7, DNAJB8,
337 DNAJB9, DNAJB12, and DNAJB14) have historically been attributed to class B due to the presence
338 of an N-terminal J-domain followed by a G/F-rich region. We used both the A/B/C and Arch12
339 classification tasks to try and reclassify these proteins. According to the A/B/C task, none of them
340 should be considered genuine class Bs. We then cross-checked this prediction with the Arch12 task.
341 We found that DNAJB12 and DNAJB14 belonged to class C and in particular to the same architectural
342 Class as DNAJC18, with whom they share the DUF1977 domain, while the other non-canonical class
343 B JDPs were predicted to belong to either class A or class B. A smaller model discriminating solely
344 class A from class B JDPs yielded consistent results (see Supplementary Table 2). Taken together, these
345 results suggest a complex evolutionary origin of the non-canonical class B JDPs, with some of them
346 possibly descending from class A JDPs (Table 1).

347 Next, we classified class C JDPs into subclasses. All original class C members were correctly predicted
348 by the A/B/C classification task. The Arch12 task also correctly classified all human class C JDPs. Of
349 note, DNAJC20 (HscB) and DNAJC23 (Sec63) (highlighted in orange in Table 1) were assigned to the
350 *Others* group, since these JDPs displayed domain architectures somewhat divergent from the Pfam-
351 annotated domains. However, the Arch12 task correctly assigned DNAJC20 and DNAJC23 to HscB
352 and Sec63 subclasses, highlighting the ability of these automated approaches to correctly annotate JDPs
353 with the help of appropriate training sets. We repeated this analysis to several other model organisms
354 covering a wide phylogenetic range, including *M. musculus*, *R. norvegicus*, *M. mulata*, *D. rerio*, *D.*
355 *melanogaster*, *C. elegans*, *A. thaliana* and *E. coli* (see Supplementary tables S3-S10).

356

357 ## Discussion

358 In the course of evolution, the JDP family expanded both in number and structural diversity, and in
359 eukaryotic organisms there is a more than two-fold increase in the number of JDPs relative to Hsp70s,
360 indicating that the limited repertoire of Hsp70 isoforms is utilized by multiple different JDPs to generate
361 various chaperoning activities (*e.g.* unfolding of misfolded protein, disassembly of functional or
362 aggregated protein oligomers, protein translocation into organelles and target proteins for degradation).
363 The assembly of different JDP-Hsp70 chaperone machines is initiated by J-domains. Genetic,
364 biochemical, and structural data accumulated over the years provide a relatively comprehensive map of
365 the J-domain-Hsp70 interface[20,21,48–53], which serves a single task, *i.e.* to establish the vital physical
366 interaction that promotes ATP hydrolysis in Hsp70[16,17,20–23] , thus allowing the chaperone to capture client
367 substrates[18]. Proper docking of the J-domain onto ATP-bound Hsp70 is ensured by a core set of
368 intermolecular contacts occurring along the helix II--loop (HDP motif)--helix III region of the J-domain,
369 which is structurally conserved from bacteria to human[20,21]. However, there is very little knowledge of
370 the regulatory elements in the J-domains that critically fine-tune this interaction[41] despite such
371 modulation being hypothesized over the years. Our ANN-based observations show the presence of
372 phylogenetic and functional signatures buried within the amino acid sequences of J-domains that appear
373 to modulate the pairing of JDPs with Hsp70s to form chaperone machines with different activities.

374 What is the basis for this functional and phylogenetic sorting? Remarkably, the most discriminative
375 sequence positions structurally coincided with the J-domain-Hsp70 binding interface, strongly hinting
376 that some amino acids have a regulatory role to optimize the selection of unique functionally specific
377 Hsp70-JDP pairs. These *in silico* observations are strongly supported by indirect experimental evidence.
378 For example, measurements of JDP stimulated ATPase activity in Hsp70s shows that J-domains are not
379 fully interchangeable with respect to their collaboration with different Hsp70s within a given species.
380 The yeast cytosol contains seven Hsp70 paralogs (Ssa1-4, Ssb1-2 & Ssz1). Both Ssa's and Ssb's bind
381 to nascent polypeptide chains to promote *de novo* protein folding. However, only the ATPase activity
382 of Ssa's, but not of Ssb's, is stimulated *in vitro* by the two major cytosolic yeast JDPs Ydj1 (class A)
383 and Sis1 (class B)[54]. This indicates that J-domains of Ydj1 and Sis1 have evolved to differentially
384 recognize these Hsp70 family members. Similarly, the ATPase activity of ER-localized yeast Hsp70
385 Bip/Kar2 (HSPA5) was shown to be induced by the J-domain of Sec63 (ER; class C) 16 times higher
386 than the J-domain of ERdj3 (ER; class C)[55] suggesting that, though both JDPs function with this Hsp70,
387 there are differences in how the two JDPs stimulate Bip for specific activities. Recent results have also
388 highlighted that, for example, the J-domain of human DNAJC27 involved in ciliogenesis, cannot be
389 substituted by almost any other human J-domain[56]. In addition, as expected, speciation also has left a
390 clearly discernible signature on the J-domain sequence, which points towards some incompatibilities in
391 JDP-Hsp70 pairing. Pairing of Hsp70s and JDPs from different organisms have generated poor
392 chaperoning activities. For example, bacterial class A JDP DnaJ stimulates the ATPase activity of

393 bacterial DnaK and human HSPA8 (Hsc70) very differently[57]. Similarly, mouse DNAJC7 (DjC7; class
394 C JDP) stimulates the ATPase activity of bacterial DnaK and murine Hsp70s (HSPA8 and HSPA5) at
395 varying levels[58] possibly leading to differences in function. Our *in silico* findings strongly suggest that
396 these incompatibilities arise from discriminatory signatures buried within the amino acid sequences of
397 J-domains. Emergence of greater sequence diversity in J-domains of JDPs, in particular at the Hsp70-
398 J-domain interaction surface, with respect to their Hsp70 partners is expected to preserve specificity in
399 pairing as the Hsp70-JDP network expanded during evolution. In general, amino acid changes at the
400 relatively small Hsp70-J-domain interaction surface would require independent compensatory
401 mutations in both the J-domain and Hsp70 to maintain compatibility. However, this is statistically very
402 unlikely, because it imposes a greater evolutionary pressure on the handful of Hsp70s (compared to the
403 large number of JDPs) in a cell. On the contrary, there is relatively less selection pressure for mutations
404 to occur on the J-domain side, but with a certain affinity cost for the pairing. As a result, we observe
405 the establishment of a gradient of interaction preferences between distinct Hsp70 and JDP pairs. This
406 largely explains the aforementioned J-domain involved Hsp70-JDP incompatibilities reported
407 experimentally. Overall, the evolution of these discriminatory genetic signatures through mutations in
408 J-domains opens the possibility to fine-tune JDP-Hsp70 interactions to support specific chaperoning
409 activities in cells.

410 Our analysis refined the JDP classification. The ANNs used show that the unique amino acid sequence
411 signatures in the J-domains also provide precise discrimination according to functional and
412 phylogenetic criteria. For example, the discriminatory signatures in the J-domains of non-canonical
413 class B JDPs (DNAJB2, DNAJB3, DNAJB6-9, DNAJB12 and DNAJB14) suggest that these JDPs are
414 very distinct from the canonical class B members such as DNAJB1, DNAJB4 and DNAJB5. This is
415 further supported by large variations in the domain architecture of the full-length proteins. The presence
416 of a G/F-rich region following the J-domain suggests that these JDPs may have evolved from a class A
417 or class B ancestor, followed by some extensive sequence divergence. Class C appears to be the largest
418 subfamily in prokaryotes[40] and has exponentially increased in number during eukaryotic evolution,
419 being further organized in subclasses that are clearly recognizable according both to their overall
420 domain architecture and to the sequences of their J-domains alone.

421 From a more general perspective, the recent advent of ANN-based approaches in structural biology,
422 epitomized by the spectacular and widely-advertised success of AlphaFold for protein structure
423 prediction[59,60], highlights that the exponentially growing number of sequences available in public
424 repositories holds a yet unexplored wealth of information that must be exploited. At the same time, this
425 data abundance also creates a problem between indiscriminate use of sequences from all sources and
426 cautious desire to use carefully curated sequences, and calls for an intermediate approach, where
427 stringent, conservative automated criteria go hand-in-hand with manual curation at higher scales (*e.g.*
428 domain composition). In this respect, the present work can be considered as an important example where

429 this strategy allows for an unbiased, semi-unsupervised coupled functional/phylogenetic-structural
430 investigation: It is supervised for the classification task, but unsupervised for the emergence of the
431 relevant structural features.

432

433 ***Limitations of the study***

434 We show here that the proposed automated classification is already possible, although likely limited
435 mostly by two factors. On the one hand, several architectural C subclasses are too poorly represented
436 in the dataset that it is difficult to train a network to tell them apart from more abundant subclasses.
437 However, this problem is likely to be solved through exponential growth of the number of reported JDP
438 sequences. On the other hand, a large swath of class C JDPs comprise domains that have not yet been
439 annotated in Pfam, or just some disordered regions of various lengths. Yet, the advent of novel deep
440 learning approaches on scales even larger than the present ones is recognizing domains that were
441 previously uncharacterized[61], paving the way for a better assignment of class C JDPs to precise, well-
442 populated architectural classes.

443

444 Methods

445 ***Construction of a curated J-protein dataset***

446 We constructed a JDP sequence database by querying the Uniprot database (union of Swissprot and
447 TrEMBL, release 2021_04)[31] to extract all sequences annotated to have a J-domain according to the
448 PFAM domain annotation (PF00226)[32]. For each JDP sequence, we recovered its full-length sequence
449 as well as the full taxonomic lineage from Uniprot. We then extracted the J-domain sequence of each
450 JDP by aligning the full-length sequences to the Hidden Markov Model (HMM) of the Pfam J-domain
451 (PF0226) family using the *hmmalign* utility of the *hmmer* package[62]. The full domain-architecture was
452 obtained by querying the PFAM database for each JDP entry in our database and the domain order
453 validated using the domain boundaries reported in PFAM.
454 The domain architectures were used to classify all sequences as either belonging to canonical class A
455 (PFAM architecture "*DnaJ;DnaJ_C;DnaJ_CXXCXGXG"*), canonical class B (PFAM architecture
456 "*DnaJ;DnaJ_C;"*) and class C (all other sequences).
457 We further identified the G/F-rich region in all JDPs as being the stretch of 40 amino-acids directly
458 following the JD sequence, if at least 25% of its amino-acids are either Glycines or Phenylalanines.
459 For ease of analysis, we also grouped all domains composing TPR repeat proteins (annotated as
460 TPR_XX) into a virtual TPR domain. Thus, in all proteins containing one or several TPR repeats, we
461 replaced all the TPR domains by a single effective TPR domain (as shown in Fig.2).
462 Subcellular localizations were predicted for eukaryotic sequences using the TargetP software[63], version
463 2.0.

464 This resulted in an initial dataset containing 232'516 annotated JDP sequences.
465 We then curated the dataset by first removing all sequences for which the Uniprot and PFAM
466 annotations were not consistent and also removed all sequences which did not have a full characteristic
467 HPD motif. We further filtered out sequences containing annotated ANTI-TRAP domains (according
468 to Pfam), because in all but one case it simply recognized the canonical ZFLR domain. Furthermore,
469 we also removed sequences containing multiple J-domains. Finally, all sequences associated to
470 unclassified organisms were also removed from our final set.
471 This resulted in a curated JDP dataset comprising 223'124 sequences.

472 ***Annotation of a novel pseudo Zinc-Finger Like Region (pseudoZFLR) domain in JDPs***

473 We created a new domain definition to annotate the pseudo zinc-finger like domains similar to the ones
474 observed in DnaJB11 and ErdJ3. These domains are characterized by one CNC and one CxxC motifs,
475 in contrast to the 4 pairs of CxxC motifs of the canonical Zinc-Finger motif as annotated in the PFAM
476 DnaJ_CXXCXGXG domain. We thus built a multiple sequence alignment containing 35 manually
477 selected and curated JDPs containing a pseudoZFLR domain, from organisms including vertebrates,
478 invertebrates and plants. We then aligned this seed using MAFFT (v7.487)[64] and manually identified a
479 region comprised of 55 positions defining the pseudoZFLR domain. We then constructed a hidden-
480 markov model profile of the novel domain using the *hmmbuild* utility from the hmmer suite[62] and used
481 to profile to query all the 223'124 JDP sequences in our curated dataset to identify JDPs containing a
482 pseudoZFLR domain. Because of the similarity between this domain and the canonical ZFLR domain,
483 we used a more stringent E-value $=10^{-4}$ cutoff to identify pseudo ZFLR domains (see Supplementary
484 Fig.7 7). This resulted in a total of 1421 JDPs identified as containing a pseudoZFLR domain, of which
485 1336 possess a DnaJ-DnaJ_C-pseudoZFLR architecture.

486 ***Dimensionality reduction of JDP amino-acid sequences by UMAP***

487 To apply the UMAP algorithm[46] to the amino-acid sequences of our J-domain repertoire for
488 visualization, we first used a one-hot-encoding technique to numerically embed the JD sequences in a
489 high-dimensional space, consisting of 63x21=1323 dimensions (20 amino-acid + 1 gap for each of the
490 63 positions in the JD aligned sequences). We then applied the UMAP dimensionality reduction
491 technique with standard parameters as provided by the original publication.

492 ***Preparation of JDP datasets for training Neural Networks***

493 To avoid training the Neural Networks on sequences for which we want to predict and interpret the
494 class labels, sequences from model organisms (*H. sapiens, M. musculus, S. cerevisiae, R. norvegicus,*
495 *melanogaster, D. rerio, C. elegans, A. thaliana*) were removed from the dataset prior to training. To
496 interpret the predictions of the trained models, we also removed non-canonical class B proteins from
497 our training set. These were identified as JDPs containing a DnaJ domain, an annotated G/F region (see
498 above) but no DnaJ_C domain. This procedure resulted in a reduced set of 205'252 sequences used for
499 building the classification models.

To reduce the effects of sampling bias during the training phase, we used as simple sequence reweighting scheme previously used in several sequence analysis pipelines[65,66]. We assigned to each sequence a weight of $1/n_{80}$, where n_{80} denotes the number of sequences with sequence identity greater than 80% from it. These weights were calculated for each classification task separately, as some tasks are only trained on a subset of sequences, which can potentially slightly modify the weights.
We randomly split the processed dataset into training, validation and test set in such a way that sequences from the same organism always belong to the same set and that the sum of the weights of each dataset is respectively 0.7, 0.15, 0.15 times that of the total.

Feed-Forward Artificial Neural Network classification

To feed the sequences to a neural network we encoded them into binary vectors. Every amino acid is mapped to an integer *A(a)* in increasing alphabetical order, with the gap symbol mapped to zero. We therefore can encode every amino acid with a 21-dimensional vector in which all elements are zeros and element *A(a)* is one (the so called *one-hot encoding*). An amino acid sequence is then obtained by concatenating all 21-dimensional vectors together. To pass the sequences to a neural network, we concatenated the one-hot encoding of each position in the alignment, resulting in a 1323-dimensional binary vector (63x21 entries).

A Dropout layer has been used between the input and first hidden layer to randomly mask a fraction of inputs and has been found to improve the generalization accuracy of the network.

For each task described in the main text, we trained a feed forward neural network to predict the corresponding label of each sequence. We trained the network by minimizing the categorical cross entropy between the output layer and the categorical encoding of the label. All weights have been regularized using an L2 regularizer. In all cases we used the Adam protocol during the minimization procedure and a learning decay equal to 0.01. A batch size of 1024 was used and SoftPlus activation were used for all hidden layers. The remaining hyperparameters (number of layers, units per layer, dropout rate, weight regularizations and initial learning rate) were optimized by performing a grid search over parameter space, testing 216 combinations of hyperparameters per task. The best performing model was selected based on the maximum accuracy on the validation set (see Table 2). The model performances are reported on the hold out test set.

After the training is completed, we analyzed the trained networks using the technique described in[47] to obtain 21x63 coefficients describing how the networks use every bit in the input in order to classify the sequence. The relevance scores for each residue is finally computed as the Frobenius norm (sum of the squares) of its corresponding elements in the coupling matrix (see[47] for details on the relevance score calculations).

534 ***Class A vs B JDP classification using unaligned G/F region sequences***

535 To test the discrimination power of the G/F regions of class A and B JDPs, we built an L_2-regularized
536 logistic regression model to classify JDPs as either belonging to class A or B. The unaligned G/F regions
537 (comprised of the 40 amino-acids following the J-domain) where one-hot encoded and fed into a
538 standard logistic regression model. The regularization parameter C has been chosen by scanning the
539 validation set accuracy (Supplementary Fig.8). The resulting best model (C=3.0) achieved classification
540 accuracy of ~95%.

541

542 ***Generate of J-protein repertoire for model organisms***

543 We built the J-protein repertoires for the following model organisms: *H. sapiens, S. cerevisiae, M.*
544 *musculus, R. norvegicus, M. mulata, D. rerio, D. melanogaster, C. elegans, A. thaliana* and *E. coli*. All
545 entries in the human, yeast and bacterial organisms were manually curated and cross-referenced with J-
546 protein repertoires of these organisms. For the remaining model organisms, we extracted all entries in
547 our dataset correspondoing to the target organism, removed entries marked as fragment and then
548 reduced redundancy by only retaining entries with both unique full-length sequences and gene names.
549 To select which Uniprot entry to keep in the tables, we prioritized entries in the annotated SwissProt
550 repository of Uniprot, and then selected the entries with the highest Uniprot annotation score.

551

552 ***Author Contributions and Notes***

553 DM and SZ conceptualized the study, prepared the dataset, performed the analysis, and wrote the
554 manuscript. MER performed the analysis, and wrote the manuscript. NBN conceptualized the study and
555 wrote the manuscript. PDLR conceptualized the study, performed the analysis, wrote the manuscript,
556 and supervised the project. AB conceptualized the study. All authors discussed the results and revised
557 the manuscript.

558

559 ***Acknowledgments***

560 DM thanks the Swiss National Science Foundation (SNFS) for financial support under grant number
561 P2ELP3_181910. NBN thanks National Health and Medical Research Council of Australia Investigator
562 Grant APP1197021 and Recruitment Grant from Monash University Faculty of Medicine Nursing and
563 Health Sciences with funding from the State Government of Victoria and the Australian Government.

564

References

1. Mandal, A. K., Nillegoda, N. B., Chen, J. A. & Caplan, A. J. Ydj1 Protects Nascent Protein Kinases from Degradation and Controls the Rate of Their Maturation. *Molecular and Cellular Biology* **28**, 4434–4444 (2008).
2. Behnke, J., Mann, M. J., Scruggs, F. L., Feige, M. J. & Hendershot, L. M. Members of the Hsp70 Family Recognize Distinct Types of Sequences to Execute ER Quality Control. *Molecular Cell* **63**, 739–752 (2016).
3. Nillegoda, N. B. *et al.* Crucial HSP70 co-chaperone complex unlocks metazoan protein disaggregation. *Nature* **524**, 247–251 (2015).
4. Wentink, A. S. *et al.* Molecular dissection of amyloid disaggregation by human HSP70. *Nature* **587**, 483–488 (2020).
5. Hageman, J. *et al.* A DNAJB chaperone subfamily with HDAC-dependent activities suppresses toxic protein aggregation. *Mol Cell* **37**, 355–69 (2010).
6. Kumar, J., Kline, N. L. & Masison, D. C. Human DnaJB6 Antiamyloid Chaperone Protects Yeast from Polyglutamine Toxicity Separately from Spatial Segregation of Aggregates. *Molecular and Cellular Biology* **38**, 1–15 (2018).
7. Sinha, D., Srivastava, S. & D'Silva, P. Functional diversity of human mitochondrial j-proteins is independent of their association with the inner membrane presequence translocase. *Journal of Biological Chemistry* **291**, 17345–17359 (2016).
8. Hassdenteufel, S. *et al.* Chaperone-Mediated Sec61 Channel Gating during ER Import of Small Precursor Proteins Overcomes Sec61 Inhibitor-Reinforced Energy Barrier. *Cell Reports* **23**, 1373–1386 (2018).
9. Li, K. *et al.* Tetrameric Assembly of K+ Channels Requires ER-Located Chaperone Proteins. *Molecular Cell* **65**, 52–65 (2017).
10. Fotin, A. *et al.* Structure of an auxilin-bound clathrin coat and its implications for the mechanism of uncoating. *Nature* **432**, 649–653 (2004).
11. Walsh, P., Bursać, D., Law, Y. C., Cyr, D. & Lithgow, T. The J-protein family: Modulating protein assembly, disassembly and translocation. *EMBO Reports* **5**, 567–571 (2004).
12. Rodriguez, F. *et al.* Molecular Basis for Regulation of the Heat Shock Transcription Factor σ32 by the DnaK and DnaJ Chaperones. *Molecular Cell* **32**, 347–358 (2008).
13. Westhoff, B., Chapple, J. P., Van Der Spuy, J., Höhfeld, J. & Cheetham, M. E. HSJ1 is a neuronal shuttling factor for the sorting of chaperone clients to the proteasome. *Current Biology* **15**, 1058–1064 (2005).
14. Grove, D. E., Fan, C. Y., Ren, H. Y. & Cyr, D. M. The endoplasmic reticulum-associated Hsp40 DNAJB12 and Hsc70 cooperate to facilitate RMA1 E3-dependent degradation of nascent CFTRΔF508. *Molecular Biology of the Cell* **22**, 301–314 (2011).
15. Yamamoto, Y. H. *et al.* ERdj8 governs the size of autophagosomes during the formation process. *Journal of Cell Biology* **219**, (2020).
16. Suh, W. C., Lu, C. Z. & Gross, C. A. Structural features required for the interaction of the Hsp70 molecular chaperone DnaK with its cochaperone DnaJ. *Journal of Biological Chemistry* **274**, 30534–30539 (1999).
17. Jiang, J. *et al.* Structural basis of J cochaperone binding and regulation of Hsp70. *Molecular Cell* **28**, 422–33 (2007).
18. De Los Rios, P. & Barducci, A. Hsp70 chaperones are non-equilibrium machines that achieve ultra-affinity by energy consumption. *Elife* **3**, e02218 (2014).
19. Bracher, A. & Verghese, J. The nucleotide exchange factors of Hsp70 molecular chaperones. *Frontiers in Molecular Biosciences* **2**, 1–9 (2015).
20. Malinverni, D., Jost Lopez, A., De Los Rios, P., Hummer, G. & Barducci, A. Modeling Hsp70/Hsp40 interaction by multi-scale molecular simulations and co-evolutionary sequence analysis. *Elife* **6**, e23471 (2017).
21. Kityk, R., Kopp, J. & Mayer, M. P. Molecular Mechanism of J-Domain-Triggered ATP Hydrolysis by Hsp70 Chaperones. *Molecular Cell* **69**, 227-237.e4 (2018).
22. Tomiczek, B. *et al.* Two-step mechanism of j-domain action in driving hsp70 function. *PLoS Computational Biology* **16**, 1–29 (2020).
23. Tsai, J. & Douglas, M. G. A conserved HPD Sequence of the J-domain Is Necessary fr YDJ1 Stimulation of Hsp70 ATPase ACtivity at a Site Distinct from Substrate Binding§. *J Biol Chem* **271**, 9347–9354 (1996).
24. Kampinga, H. & Craig, E. The HSP70 chaperone machinery: J proteins as drivers of functional specificity. *Nature Reviews. Molecular Cell Biology* **11**, 579–92 (2010).
25. Craig, E. A. & Marszalek, J. How Do J-Proteins Get Hsp70 to Do So Many Different Things? *Trends in Biochemical Sciences* **42**, 355–368 (2017).
26. Rajan, V. B. V. & D'Silva, P. Arabidopsis thaliana J-class heat shock proteins: Cellular stress sensors. *Functional and Integrative Genomics* **9**, 433–446 (2009).
27. Cheetham, M. E. & Caplan, A. J. Structure, function and evolution of DnaJ: Conservation and adaptation of chaperone function. *Cell Stress and Chaperones* vol. 3 28–36 Preprint at https://doi.org/10.1379/1466-1268(1998)003<0028:SFAEOD>2.3.CO;2 (1998).
28. Zhang, R., Malinverni, D., Cyr, D. M., Rios, P. D. L. & Nillegoda, N. B. J-domain protein chaperone circuits in proteostasis and disease. *Trends in Cell Biology* 1–18 (2022) doi:10.1016/j.tcb.2022.05.004.
29. Jiang, Y., Rossi, P. & Kalodimos, C. G. Structural basis for client recognition and activity of Hsp40 chaperones. *Science (1979)* **365**, 1313–1319 (2019).
30. Baaklini, I. *et al.* The DNAJA2 substrate release mechanism is essential for chaperone-mediated folding. *Journal of Biological Chemistry* **287**, 41939–41954 (2012).
31. Bateman, A. *et al.* UniProt: The universal protein knowledgebase. *Nucleic Acids Research* **45**, D158–D169 (2017).
32. Mistry, J. *et al.* Pfam: The protein families database in 2021. *Nucleic Acids Research* **49**, D412–D419 (2021).

33. Ottaviani, D. *et al.* Protein kinase CK2 modulates HSJ1 function through phosphorylation of the UIM2 domain. *Human Molecular Genetics* **26**, 611–623 (2017).
34. Howarth, J. L. *et al.* Hsp40 molecules that target to the ubiquitin-proteasome system decrease inclusion formation in models of polyglutamine disease. *Molecular Therapy* **15**, 1100–1105 (2007).
35. Ryder, B. D. *et al.* Regulatory inter-domain interactions influence Hsp70 recruitment to the DnaJB8 chaperone. *Nature Communications* **12**, 1–16 (2021).
36. Faust, O. *et al.* HSP40 proteins use class-specific regulation to drive HSP70 functional diversity. *Nature* **587**, 489–494 (2020).
37. Yu, H. Y., Ziegelhoffer, T. & Craig, E. a. Functionality of Class A and Class B J-protein co-chaperones with Hsp70. *FEBS Letters* 1–6 (2015) doi:10.1016/j.febslet.2015.07.040.
38. Karamanos, T. K., Tugarinov, V. & Clore, G. M. Unraveling the structure and dynamics of the human DNAJB6b chaperone by NMR reveals insights into Hsp40-mediated proteostasis. *Proc Natl Acad Sci U S A* **116**, 21529–21538 (2019).
39. Gu, J. *et al.* Hsp40 proteins phase separate to chaperone the assembly and maintenance of membraneless organelles. *Proc Natl Acad Sci U S A* **117**, 31123–31133 (2020).
40. Barriot, R., Latour, J., Castanié-Cornet, M. P., Fichant, G. & Genevaux, P. J-Domain Proteins in Bacteria and Their Viruses. *Journal of Molecular Biology* **432**, 3771–3789 (2020).
41. Hennessy, F., Nicoll, W. S., Zimmermann, R., Cheetham, M. E. & Blatch, G. L. Not all J domains are created equal: implications for the specificity of Hsp40-Hsp70 interactions. *Protein Sci* **14**, 1697–709 (2005).
42. Qiu, X.-B., Shao, Y.-M., Miao, S. & Wang, L. The diversity of the DnaJ/Hsp40 family, the crucial partners for Hsp70 chaperones. *Cell Mol Life Sci* **63**, 2560–70 (2006).
43. Kluck, C. J. *et al.* Structure-function analysis of HscC, the Escherichia coli member of a novel subfamily of specialized Hsp70 chaperones. *J Biol Chem* **277**, 41060–9 (2002).
44. Schlenstedt, G., Harris, S., Risse, B., Lill, R. & Silver, P. A. A yeast DnaJ homologue, Scj1p, can function in the endoplasmic reticulum with BiP/Kar2p via a conserved domain that specifies interactions with Hsp70s. *Journal of Cell Biology* **129**, 979–988 (1995).
45. Sullivan, C. S., Cantalupo, P. & Pipas, J. M. The Molecular Chaperone Activity of Simian Virus 40 Large T Antigen Is Required To Disrupt Rb-E2F Family Complexes by an ATP-Dependent Mechanism. *Molecular and Cellular Biology* **20**, 6233–6243 (2000).
46. McInnes, L., Healy, J. & Melville, J. UMAP: Uniform Manifold Approximation and Projection for Dimension Reduction. (2018).
47. Zamuner, S. & de Los Rios, P. Interpretable Neural Networks based classifiers for categorical inputs. *Arxiv* (2021).
48. Gässler, C. S. *et al.* Mutations in the DnaK chaperone affecting interaction with the DnaJ cochaperone. *Biochemistry* **95**, 15229–15234 (1998).
49. Greene, M. K., Maskos, K. & Landry, S. J. Role of the J-domain in the cooperation of Hsp40 with Hsp70. *Proc Natl Acad Sci U S A* **95**, 6108–13 (1998).
50. Suh, W. C. *et al.* Interaction of the Hsp70 molecular chaperone, DnaK, with its cochaperone DnaJ. *Proc Natl Acad Sci U S A* **95**, 15223–8 (1998).
51. Wittung-Stafshede, P., Guidry, J., Horne, B. E. & Landry, S. J. The J-domain of Hsp40 couples ATP hydrolysis to substrate capture in Hsp70. *Biochemistry* **42**, 4937–4944 (2003).
52. Landry, S. J. Structure and energetics of an allele-specific genetic interaction between dnaJ and dnaK: correlation of nuclear magnetic resonance chemical shift perturbations in the J-domain of Hsp40/DnaJ with binding affinity for the ATPase domain of Hsp70/DnaK. *Biochemistry* **42**, 4926–36 (2003).
53. Barducci, A. & De Los Rios, P. Non-equilibrium conformational dynamics in the function of molecular chaperones. *Current Opinion in Structural Biology* **30**, 161–169 (2015).
54. Lopez-Buesa, P., Pfund, C. & Craig, E. A. The biochemical properties of the ATPase activity of a 70-kDa heat shock protein (Hsp70) are governed by the C-terminal domains. *Proc Natl Acad Sci U S A* **95**, 15253–15258 (1998).
55. Vembar, S. S., Jin, Y., Brodsky, J. L. & Hendershot, L. M. The mammalian Hsp40 ERdj3 requires its Hsp70 interaction and substrate-binding properties to complement various yeast Hsp40-dependent functions. *Journal of Biological Chemistry* **284**, 32462–32471 (2009).
56. Piette, B. L. *et al.* Comprehensive interactome profiling of the human Hsp70 network highlights functional differentiation of J domains. *Molecular Cell* **81**, 2549-2565.e8 (2021).
57. Minami, Y., Höhfeld, J., Ohtsuka, K. & Hartl, F. U. Regulation of the heat-shock protein 70 reaction cycle by the mammalian DnaJ homolog, Hsp40. *Journal of Biological Chemistry* **271**, 19617–19624 (1996).
58. Kroczynska, B. & Blond, S. Y. Cloning and characterization of a new soluble murine J-domain protein that stimulates BiP, Hsc70 and DnaK ATPase activity with different efficiencies. *Gene* **273**, 267–274 (2001).
59. Jumper, J. *et al.* Highly accurate protein structure prediction with AlphaFold. *Nature* (2021) doi:10.1038/s41586-021-03819-2.
60. Tunyasuvunakool, K. *et al.* Highly accurate protein structure prediction for the human proteome. *Nature* **596**, 590–596 (2021).
61. Bileschi, M. L. *et al.* Using deep learning to annotate the protein universe. *Nat Biotechnol* (2022) doi:10.1038/s41587-021-01179-w.
62. Finn, R. D., Clements, J. & Eddy, S. R. HMMER web server: Interactive sequence similarity searching. *Nucleic Acids Research* **39**, 29–37 (2011).
63. Armenteros, J. J. A. *et al.* Detecting sequence signals in targeting peptides using deep learning. *Life Science Alliance* **2**, 1–14 (2019).

64. Katoh, K., Misawa, K., Kuma, K. & Miyata, T. MAFFT: a novel method for rapid multiple sequence alignment based on fast Fourier transform. *Nucleic Acids Res* **30**, 3059–3066 (2002).
65. Morcos, F., Hwa, T., Onuchic, J. N. & Weigt, M. Direct Coupling Analysis for Protein Contact Prediction. in *Protein Structure Prediction* (ed. Kihara, D.) 55–70 (Springer New York, 2014). doi:10.1007/978-1-4939-0366-5_5.
66. Ekeberg, M., Lövkvist, C., Lan, Y., Weigt, M. & Aurell, E. Improved contact prediction in proteins: Using pseudolikelihoods to infer Potts models. *Physical Review E* **87**, 012707 1–16 (2013).

704 # Tables

Table 1. Classification of the 50 *H. sapiens* JDPs. Architectures grouped into the "Other" class are indicated by *(Other)* in the third column. Class C JDPs mis-predicted in the Arch12 task are highlighted in orange: DNAJC20 is actually recognized as a HscB class C protein, although the presence of further domains in the human homolog makes the classification formally wrong; a similar argument applies to DNAJCC23 (SEC63). The presence of corrupted HPDs (*e.g.* DNAJB13) does not change the classification based on the J-domain, because all J-domains used in the training of the Arch12 ANN had a canonical HPD motif. As a consequence, those positions are immaterial to the classification. For non-canonical class B JDPs, we report in green the modified nomenclature introduced in[28]. The reference proteome (UP000005640 (Homo sapiens)) was used to perform the search of the JDPs.

	***H. Sapiens* name**	**Uniprot**	**Domain Architecture *(Ground truth)***	**A/B/C Probabilities**	**Arch12 Probabilities**
	Class A				
1	DNAJA1	P31689	DnaJ - DnaJ_C - DnaJ_CXXCXGXG	**0.94** / 0.06 / 0.00	DnaJ;DnaJ_C;DnaJ_CXXCXGXG **(0.98)**
2	DNAJA2	O60884	DnaJ - DnaJ_C - DnaJ_CXXCXGXG	**1.00** / 0.00 / 0.00	DnaJ;DnaJ_C;DnaJ_CXXCXGXG **(1.0)**
3	DNAJA3	Q96EY1	DnaJ - DnaJ_C - DnaJ_CXXCXGXG	**0.99** / 0.00 / 0.00	DnaJ;DnaJ_C;DnaJ_CXXCXGXG **(0.97)**
4	DNAJA4	Q8WW22	DnaJ - DnaJ_C - DnaJ_CXXCXGXG	**0.89** / 0.10 / 0.01	DnaJ;DnaJ_C;DnaJ_CXXCXGXG **(0.96)**
	Canonical Class B				
5	DNAJB1	P25685	DnaJ - DnaJ_C	0.00 / **1.00** / 0.00	DnaJ;DnaJ_C **(0.98)**
6	DNAJB4	Q9UDY4	DnaJ - DnaJ_C	0.00 / **1.00** / 0.00	DnaJ;DnaJ_C **(1.0)**
7	DNAJB5	O75953	DnaJ - DnaJ_C	0.00 / **0.99** / 0.01	DnaJ;DnaJ_C **(0.98)**
8	DNAJB11	Q9UBS4	DnaJ - DnaJ_C - pseudoZFLR *(Other)*	0.00 / 0.04 / **0.96**	Other **(0.89)**
9	DNAJB13 (not HPD)	P59910	DnaJ - DnaJ_C	0.00 / 0.01 / **0.99**	DnaJ;DnaJ_C **(0.77)**
	Non-canonical Class B				
10	DNAJB2 (DNAJC31)	P25686	DnaJ	0.00 / 0.03 / **0.96**	DnaJ;DnaJ_C **(0.92)**
11	DNAJB3 (DNAJC32)	Q8WWF6	DnaJ	**0.45** / 0.11 / 0.44	DnaJ;DnaJ_C **(0.62)**
12	DNAJB6 (DNAJC33)	O75190	DnaJ	**0.58** / 0.05 / 0.37	DnaJ;DnaJ_C;DnaJ_CXXCXGXG **(0.63)**
13	DNAJB7 (DNAJC34)	Q7Z6W7	DnaJ	**0.76** / 0.11 / 0.14	DnaJ;DnaJ_C;DnaJ_CXXCXGXG **(0.79)**
14	DNAJB8 (DNAJC35)	Q8NHS0	DnaJ	0.03 / 0.01 / **0.97**	DnaJ;DnaJ_C;DnaJ_CXXCXGXG **(0.58)**
15	DNAJB9 (DNAJC36)	Q9UBS3	DnaJ	0.12 / 0.00 / **0.88**	DnaJ;DnaJ_C;DnaJ_CXXCXGXG **(0.82)**
16	DNAJB12 (DNAJC37)	Q9NXW2	DnaJ - DUF1977	0.03 / 0.00 / **0.96**	DnaJ;DUF1977 **(1.0)**
17	DNAJB14 (DNAJC38)	Q8TBM8	DnaJ - DUF1977	0.00 / 0.00 / **1.00**	DnaJ;DUF1977 **(1.0)**
	Class C				
18	DNAJC1	Q96KC8	DnaJ - Myb_DNA-binding *(Other)*	0.00 / 0.00 / **1.00**	Other **(1.0)**
19	DNAJC2	Q99543	DnaJ – RAC_head - Myb_DNA-binding - Myb_DNA-binding *(Other)*	0.00 / 0.00 / **1.00**	Other **(1.0)**
20	DNAJC3	Q13217	TPR_16 – TPR1 – TPR_8 - DnaJ	0.00 / 0.00 / **1.00**	DnaJ;TPR **(1.0)**
21	DNAJC4	Q9NNZ3	DnaJ	0.00 / 0.00 / **1.00**	Other **(1.0)**
22	DNAJC5	Q9H3Z4	DnaJ	0.00 / 0.01 / **0.99**	Other **(0.97)**
23	DNAJC5B	Q9UF47	DnaJ	0.00 / 0.00 / **1.00**	Other **(0.63)**
24	DNAJC5G	B5MCA9	DnaJ	0.00 / 0.00 / **1.00**	Other **(0.98)**
25	DNAJC6 (AUXILIN)	O75061	PTEN_C2 – DnaJ *(Other)*	0.00 / 0.00 / **1.00**	Other **(1.0)**
26	DNAJC7	Q99615	TPR_11 – TPR_16 – TPR_8 - DnaJ	0.02 / 0.03 / **0.95**	DnaJ;TPR **(1.0)**
27	DNAJC8	O75937	DnaJ	0.00 / 0.00 / **1.00**	Other **(1.0)**
28	DNAJC9	Q8WXX5	DnaJ	0.00 / 0.00 / **1.00**	Other **(1.0)**
29	DNAJC10	Q8IXB1	DnaJ – Thioredoxin - Thioredoxin - Thioredoxin - Thioredoxin *(Other)*	0.00 / 0.00 / **1.00**	Other **(0.99)**
30	DNAJC11	Q9NVH1	DnaJ - DnaJ-like_C11_C	0.00 / 0.00 / **1.00**	DnaJ;DnaJ-like_C11_C **(1.0)**
31	DNAJC12	Q9UKB3	DnaJ	0.00 / 0.00 / **1.00**	Other **(1.0)**
32	DNAJC13	O75165	RME-8_M - GYF_2 - DnaJ *(Other)*	0.00 / 0.00 / **1.00**	Other **(1.0)**
33	DNAJC14	Q6Y2X3	DnaJ - Jiv90 *(Other)*	0.00 / 0.00 / **1.00**	Other **(1.0)**
34	DNAJC15	Q9Y5T4	DnaJ	0.00 / 0.00 / **1.00**	Other **(1.0)**
35	DNAJC16	Q9Y2G8	DnaJ - Thioredoxin	0.05 / 0.03 / **0.92**	Other **(0.61)**
36	DNAJC17	Q9NVM6	DnaJ - RRM_1 *(Other)*	0.00 / 0.00 / **1.00**	Other **(1.0)**
37	DNAJC18	Q9H819	DnaJ - DUF1977	0.00 / 0.00 / **1.00**	DnaJ;DUF1977 **(1.0)**
38	DNAJC19 (TIM14)	Q96DA6	DnaJ	0.00 / 0.00 / **1.00**	Other **(1.0)**
39	DNAJC20 (HSCB)	Q8IWL3	HscB_4_cys - DnaJ - HSCB_C	0.00 / 0.00 / **1.00**	DnaJ;HSCB_C **(0.99)**
40	DNAJC21	Q5F1R6	DnaJ - zf-C2H2_jaz	0.00 / 0.00 / **1.00**	DnaJ;zf-C2H2_jaz **(1.0)**
41	DNAJC22	Q8N4W6	TM2 – DnaJ *(Other)*	0.00 / 0.00 / **1.00**	Other **(1.0)**
42	DNAJC23 (SEC63)	Q9UGP8	DnaJ - Sec63 - Sec63 *(Other)*	0.00 / 0.00 / **1.00**	DnaJ;Sec63 **(0.97)**
43	DNAJC24	Q6P3W2	DnaJ - zf-CSL	0.00 / 0.00 / **1.00**	DnaJ;zf-CSL **(1.0)**

44	DNAJC25	Q9H1X3	DnaJ	0.00 / 0.00 / **1.00**	Other **(0.95)**
45	DNAJC25-GNG10	A0A024R161	DnaJ - G-gamma *(Other)*	0.00 / 0.00 / **1.00**	Other **(0.98)**
46	DNAJC26 (GAK)	O14976	Pkinase - PTEN_C2 – DnaJ *(Other)*	0.00 / 0.00 / **1.00**	Other **(1.0)**
47	DNAJC27	Q9NZQ0	Ras – DnaJ *(Other)*	0.00 / 0.00 / **1.00**	Other **(1.0)**
48	DNAJC28	Q9NX36	DnaJ – DJC28_CD *(Other)*	0.00 / 0.00 / **1.00**	Other **(1.0)**
49	DNAJC29 (SACSIN)	Q9NZJ4	Ubiquitin – DnaJ – HEPN *(Other)*	0.00 / 0.00 / **1.00**	Other **(0.98)**
50	DNAJC30	Q96LL9	DnaJ	0.00 / 0.00 / **1.00**	DnaJ;DnaJ-X **(1.0)**

705

706 **Table 2. Optimal hyperparameters used for training the different classification networks.**
707

Task	Layers	Units	Kernel/Bias regularization	Learning Rate	Dropout
AB	4	128,128,128,128	0.0000001	0.3	0.2
ABC	2	128,128	0.000001	0.5	0.2
Localization	4	128,128,128,128	0.000001	0.3	0.2
Phylo	2	128,128	0.000001	0.5	0.2
Bac/Euk/Arch/Vir	4	128,128,128,128	0.00001	0.4	0.2
Top12Archs	4	128,128,128,128	0.00001	0.4	0.1

708
709
710

711 **Figures**

712

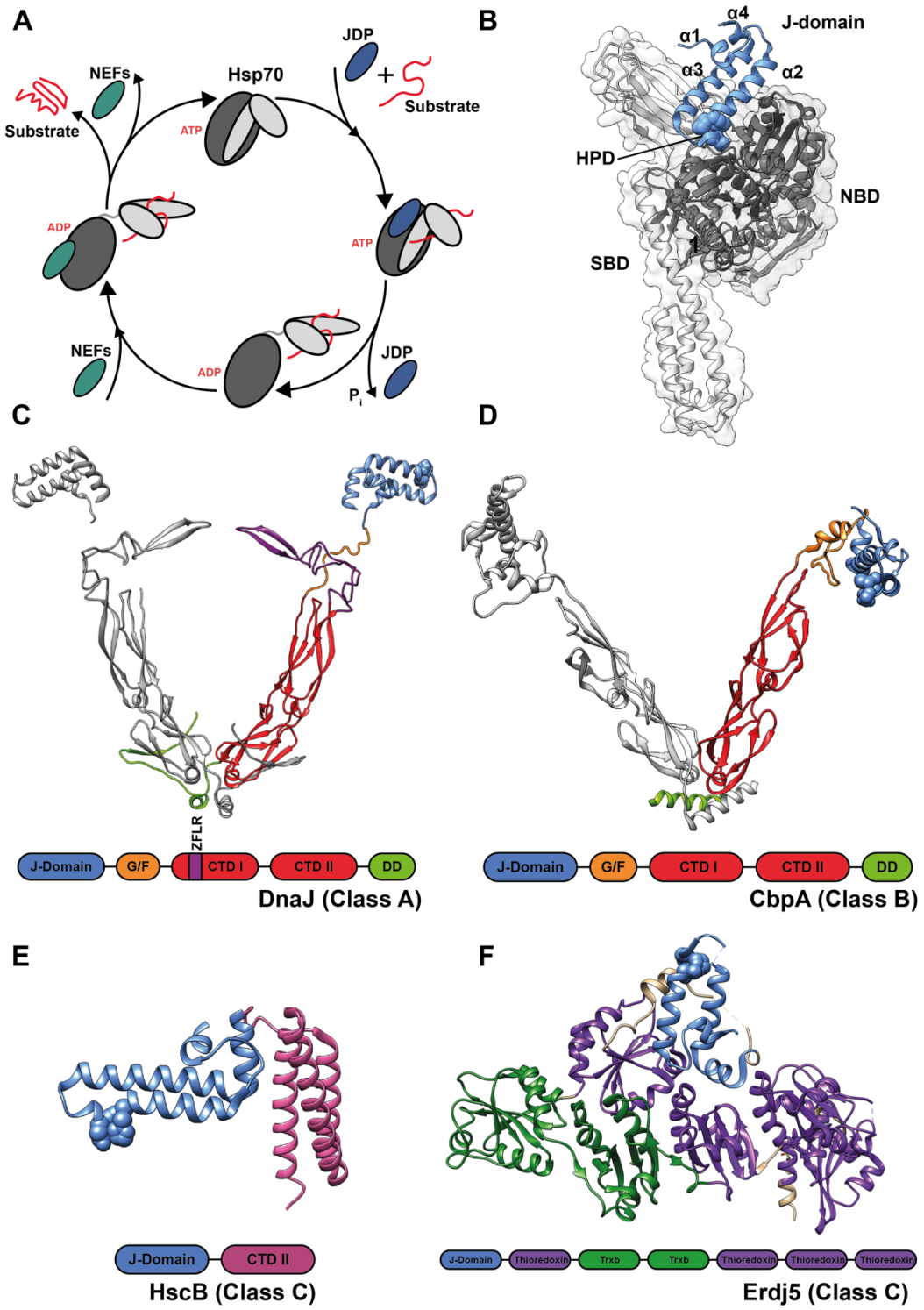

713

714 **Figure 1. Structural views of the J-domain and domain architectures of JDPs. A)** Schematic view
715 of the canonical Hsp70 cycle. **B)** Structural view of the Hsp70-J-domain complex (PDB ID: 5NRO).
716 NBD denotes the Hsp70 Nucleotide Binding Domain, SBD the Hsp70 Substrate Binding Domain. The
717 four helices (α1-α4) forming the J-domain and the characteristic HPD motif are highlighted. **C)**
718 Cytosolic class A JDP of *S. cerevisiae* (Ydj1) in its constitutive homo-dimeric form (the structure is a

719 combination of the separate J-domain, PDB ID 5VSO, CTDs PDB ID 1NLT, and dimerization domains,
720 PDB ID 1XAO); in lack of a known experimentally determined structure, the G/F rich linker between
721 the J-domain and the first C-terminal domain has been hand-drawn on one of the two protomers. The
722 different domains have been colored only on one protomer. The general architecture of class A JDPs is
723 highlighted below the structure (G/F: glycine/phenylalanine rich linker; CTD: C-terminal, substrate
724 binding domain; ZFLR: cysteine-rich, Zinc-Finger-Like Region; DD: dimerization domain). **C)** Class
725 B JDP of *Thermus thermophilus* in its constitutive homo-dimeric form (PDB ID 1C3G). The different
726 domains have been colored only on one protomer. The general architecture of class B JDPs is
727 highlighted below the structure. **D)** *Escherichia coli* HscB (class C; PDB ID 1FPO) with its architecture
728 (HSCB-C: C-terminal domain of HscB). **E)** *Mus musculus* Erdj5 (class C; PDB ID 5AYK) and its
729 architecture.
730

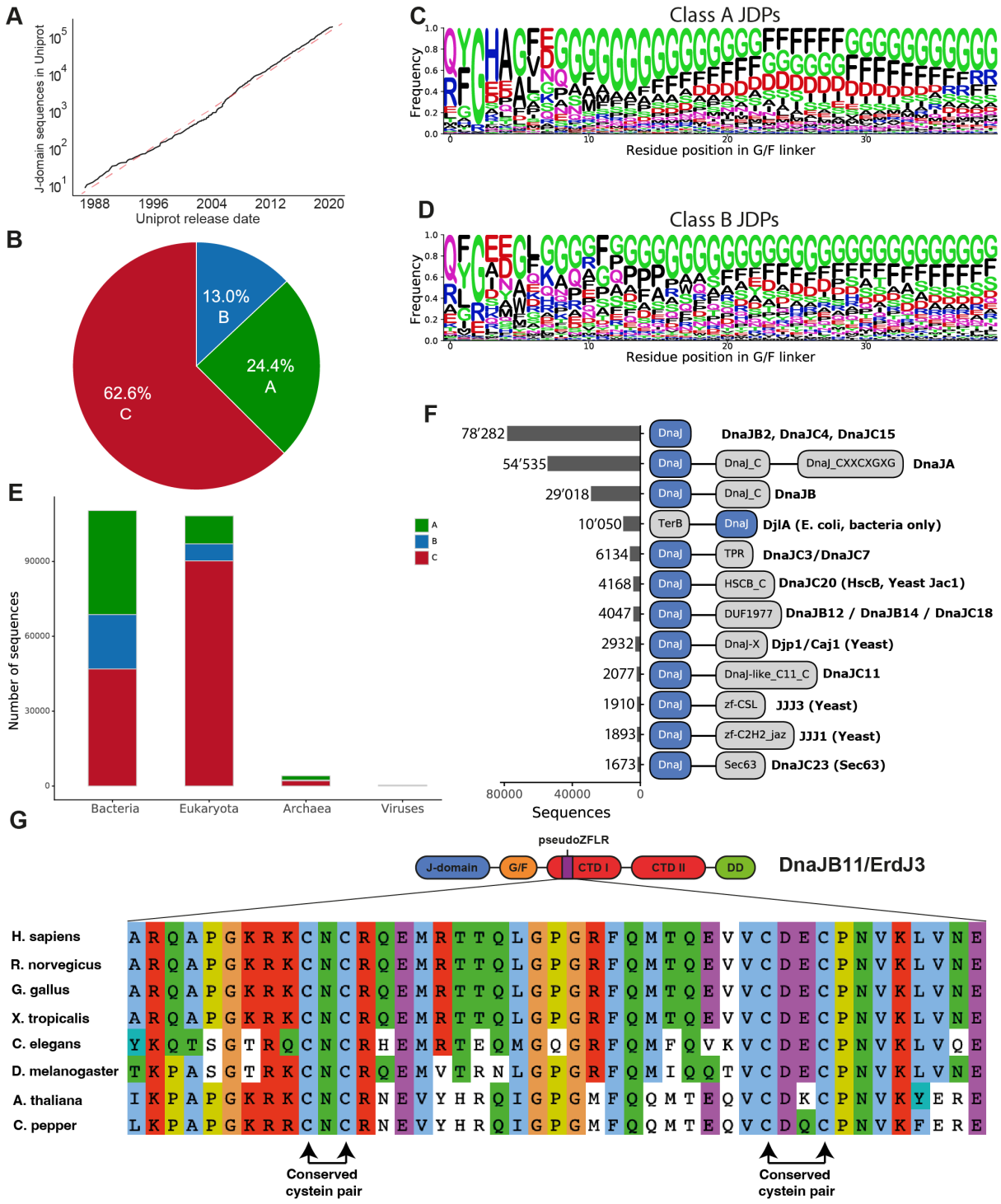

Figure 2. JDP dataset characterization. A) Growth of the number of JDP sequences found in the Uniprot Database over the last 3 decades. The red dashed line shows an exponential fit. **B)** Class proportions in the dataset. **C)** Amino-acid frequencies of the G/F linker region of class A JDPs. **D)** Amino-acid frequencies of the G/F linker region of class B JDPs. **E)** Number of JDPs in the different kingdoms, highlighted by their class (A: green; B: blue; C: red). **F)** The 12 most abundant J-protein domain architectures. Numbers on the left denote the number of sequences with this architecture in our dataset, and, on the right, we report the corresponding human, yeast, plant or bacterial proteins. **G)**

740 Highlight of the evolutionary conservation of the cysteine-rich proto-ZFLR in ER-resident JDPs in 6
741 metazoa and 2 plants.
742
743

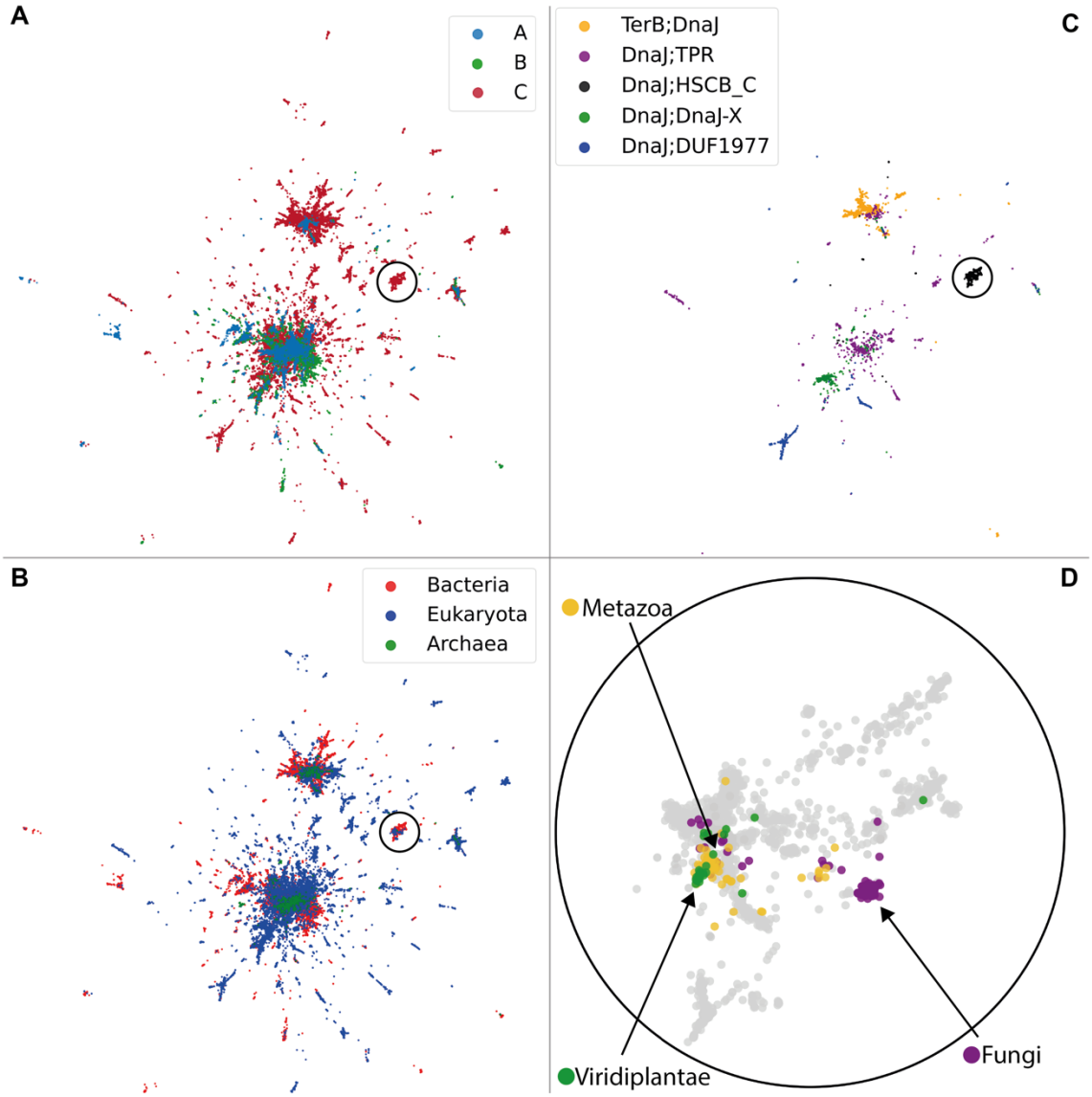

Figure 3. Two-dimensional UMAP representations of J-domains. JDP sequences are projected in two dimensions by a non-linear transformation (UMAP) and colored according to different schemes. **A)** J-domains are identified as being of class A (green), B (blue) or C (red) JDPs. **B)** J-domains are identified as being of bacterial (red) or eukaryotic (blue) origin. **C)** The five most abundant C subclasses are highlighted (see Fig.2F for representative members). The circles in each panel focus on the group identified as HscB-like JDPs. **D)** Zoom on the encircled region in the 3 other panels, highlighting the further differentiation of the eukaryotic ones into fungi, metazoa and plants (bacterial HscB sequences are shown in grey background). For visual clarity, a random subset of 50% of all points are displayed.

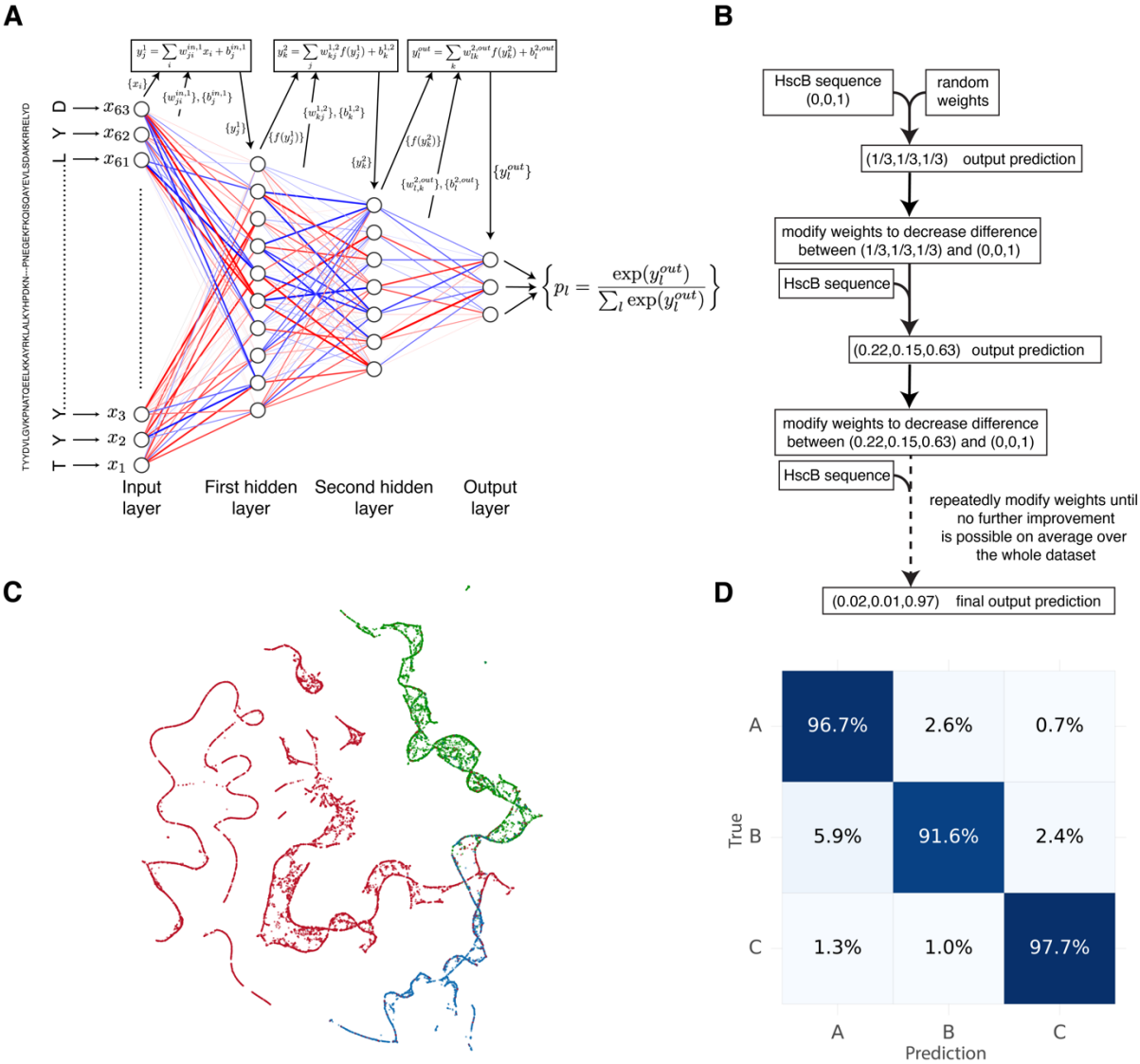

Figure 4. Structure, training and interpretation of Artificial Neural Networks. A) Structure of an ANN composed by input and output layers, separated by hidden layers (in this examples, two hidden layers); each node of a layer receives as input linear combinations of the values contained in the nodes of the previous layer, applies to them a non-linear function and the procedure is then repeated toward the next layer; the output layer transforms the received values into the probabilities for the input to belong to the various classes that must be distinguished. For visual clarity, the one-hot-encoding of the input sequences is not shown. The actual input size of all networks is 63*21=1323. **B)** Outline of the iterative procedure to change the ANN weights so that, on average over the training set, sequences are assigned as correctly as possible to their ground-truth class (defined according to domain composition). **C)** Two-dimensional embedding of the learnt probabilities for each J-domain sequence for the A *vs.* B *vs.* C classification task (colors according to the ground truth), providing a pictorial representation of

the quality of the distinction of the classes. **D)** Confusion matrix for the A *vs.* B *vs.* C classification task: each entry tells what fraction of a given class is classified to the possible classes, providing an intuitive appraisal of the ANN performance.

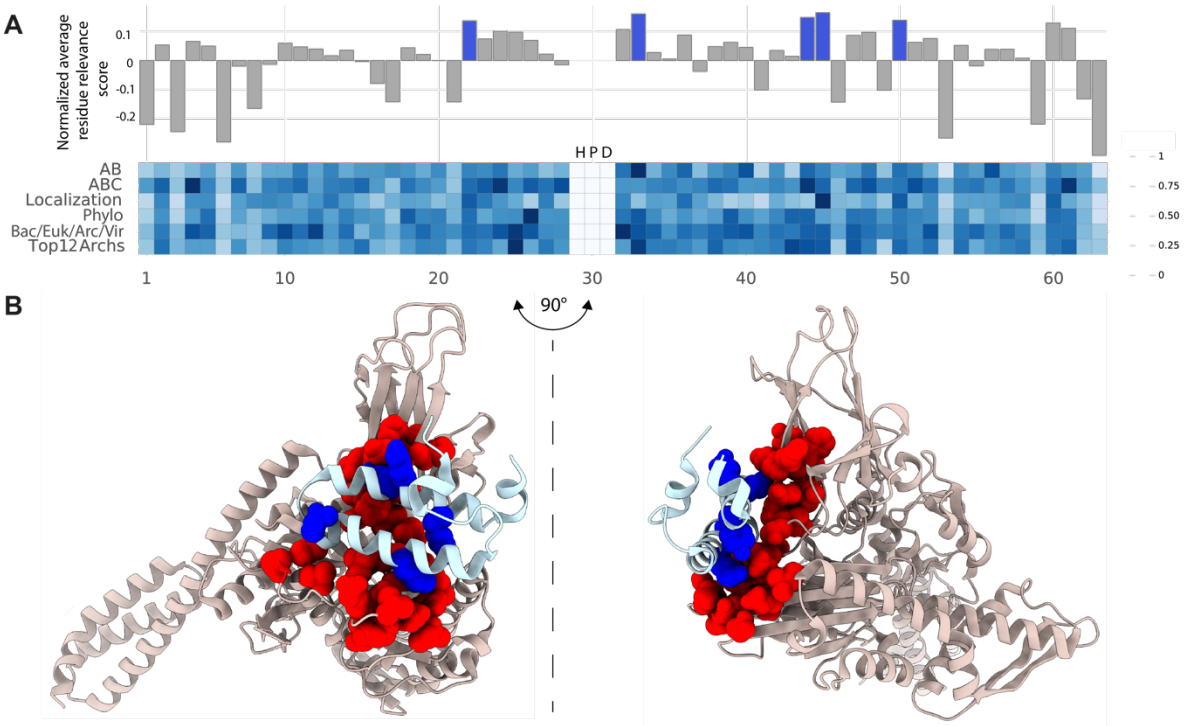

Figure 5. Identification of the most sequence and structure positions relevant for the classification. A) The relevance score for each position and for different classification tasks is represented in a heatmap. For each position, the relevance score averaged over the different tasks is represented, relative to the average over all positions, above the heatmap (HPD are not considered as they are completely irrelevant for all tasks). The top five positions are highlighted in blue. **B)** The five top scores identified in the top panel are highlighted in blue on the structure of the J-domain/DnaK complex[21], while the corresponding contacting residues on DnaK are represented in red, showing that the five most relevant positions on the J-domain participate in the interaction surface between the two proteins.